Integral imaging with improved depth of field by use of amplitude-modulated microlens arrays

Manuel Martínez-Corral, Bahram Javidi, Raúl Martínez-Cuenca, and Genaro Saavedra

One of the main challenges in three-dimensional integral imaging is its limited depth of field. Such a limitation is imposed by diffraction, among other factors. The easiest way to improve the depth of field is by reducing the numerical aperture of the microlenses. However, such an improvement is obtained at the expense of an important deterioration in the spatial resolution. We propose a technique, which is novel in the context of integral imaging, for improving the depth of field with no deterioration of the spatial resolution. The technique, based on amplitude modulation of the array of phase elements, can substantially improve the figure of merit of the product of depth of the focus and the squared resolution.

OCIS codes: 110.6880, 110.4190, 350.5730.

1. Introduction

Integral imaging is a promising three-dimensional (3D) imaging technique that provides autostereoscopic images from a continuous viewpoint and does not require the use of any special glasses.[1–6] Although integral photography was first proposed by Lippmann in 1908,[1] there has been recent interest in it because of its application to 3D TV and visualization.[7] The term integral imaging was introduced to reflect the imaging and the image-processing nature for modern applications.[8,9] In an integral-imaging system, a two-dimensional (2D) array of 2D elemental images of a given surface 3D object is generated by a microlens array and recorded on a CCD. Any elemental image shows a different perspective of the 3D object. The recorded 2D elemental images are displayed by an optical device, such as a LCD, in front of another microlens array to reconstruct the 3D image. Since its rebirth in 1997 by Okano *et al.*,[10] many important theoretical and experimental contributions to integral imaging have been reported.[11–18]

Three-dimensional integral-imaging systems still face some problems. One issue is the limited depth of field. In a typical scene objects exist at different depth positions. Since only a single plane is used to capture the images, it is not possible for all objects to be in focus. Then blurred images of objects, or parts of objects, that are out of focus are obtained. Although the depth of field of integral-imaging systems is influenced by many parameters (related to both the capture and the display systems), it is apparent that to display a clear integral image of an axially elongated 3D object it is essential to capture sharp 2D elemental images of it. For this reason the bottleneck of the depth of field in integral imaging is the limited depth of field of the microlens array used in the pickup stage. One could overcome this problem by reducing the numerical aperture (NA) of the lenses. However, such a reduction would produce as a collateral effect an important worsening of the lateral resolution of the capture stage and therefore of the spatial resolution of the overall integral-imaging system. In the past few years some new alternative techniques have been proposed to improve the depth of field of the integral-imaging systems. These methods are based on the synthesis of real and virtual image fields,[19] or on the use of lenses with nonuniform focal lengths and aperture sizes.[20,21]

In this paper we propose a new method for producing a significant enlargement of the depth of field of the integral-imaging pickup system. This enlargement is not accompanied by a deterioration of spatial resolution. The method, whose main feature is its simplicity, is based on an adequate binary modula-

M. Martinez and B. Javidi (bahram@engr.uconn.edu) are with the Department of Electrical and Computer Engineering, University of Connecticut, Storrs, Connecticut 06269-1157. R. Martinez-Cuenca and G. Saavedra are with the Department of Optics, University of Valencia, E-46100 Burjassot, Spain.

Received 14 November 2003; revised manuscript received 14 June 2004; accepted 6 July 2004.

0003-6935/04/315806-08$15.00/0

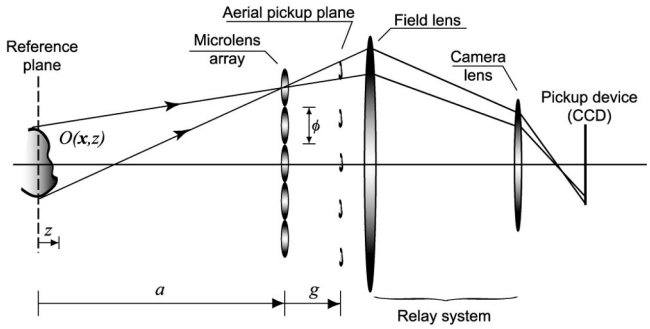

Fig. 1. Schematic, not to scale, of the capture setup of a 3D integral-imaging system. The points of the surface object $O(\mathbf{x}, z)$ out of the reference plane produce blurred images in the aerial pickup plane and therefore on the CCD. In the relay system the field lens collects the rays proceeding from the outermost microlenses, and the camera lens projects the images onto the CCD.

tion of the amplitude transmittance of the microlenses.

To present our technique, we start by carrying out a theoretical analysis of the pickup stage of the integral-imaging systems in terms of the scalar diffraction theory. This analysis explicitly takes into account, for the first time we believe, the fact that the object is a surface object. This assumption allows us to develop a set of equations [Eqs. (1)–(7)] that constitutes a strict description of the diffractional behavior of the pickup of an integral-imaging system. This analysis shows us that, conversely to what is generally assumed, integral-imaging systems are not linear and shift invariant, and therefore it is not valid *stricto senso* to define either a point-spread function or an optical transfer function. Our second step is to design an adequate amplitude modulator that should be applied to any element of the microlens array. We have performed a numerical simulation with a computer-synthesized object to show that the depth of focus shows important improvement.

2. Theoretical Analysis of the Capture Stage

To discuss the method we start by describing the capture stage from the point of view of diffraction theory. Note that since the microlens arrays generally used in integral-imaging experiments are of low NA ($NA \approx 0.2$), the analysis can be accurately performed within the frame of the paraxial scalar diffraction theory. In Fig. 1 we show the capture setup. Spatial coordinates are denoted $\mathbf{x} = (x, y)$ and z for directions transverse and parallel to the system's main optical axis. We consider a surface object under spatially incoherent illumination. For simplicity we assume, in the first stage of our formulation, a quasi-monochromatic illumination with mean wavelength λ. Light emitted by the surface object is collected by the microlens array to form a collection of 2D elemental aerial images. The images are in the so-called aerial pickup plane, which is set at a distance g from the microlens array. The reference and the aerial pickup plane are conjugated through the microlenses so that distances a and g are related by the lens law, $1/a + 1/g - 1/f = 0$. Any elemental image shows a different perspective of the surface object. In our scheme a relay system, composed by a field lens and a camera lens, is used to image the aerial images into the pickup device (usually a CCD camera). The lateral magnification of the relay system is adjusted so that the size of the collection array of the elemental images matches the CCD.

The intensity distribution of incoherent light scattered by the object can be represented by the real and positive function:

$$O(\mathbf{x}, z) = R(\mathbf{x})\delta[z - f(\mathbf{x})], \tag{1}$$

where function $R(\mathbf{x})$ accounts for the object intensity reflectivity, whereas $f(\mathbf{x}) - z = 0$ is the function that describes the surface.

We consider now the light scattered at an arbitrary point $(\mathbf{x}, z)$ of the surface object. It is straightforward, by application in the cascade of paraxial scalar diffraction equations, to find that the intensity at a given point $\mathbf{x}' = (x', y')$ of the aerial pickup plane is given by

$$H_\lambda(\mathbf{x}'; \mathbf{x}, z) = \left| \sum_{\mathbf{m}} \exp\left[i \frac{\pi}{\lambda(a - z)} |\mathbf{m}p - \mathbf{x}|^2 \right] \int \mathsf{P}_z(\mathbf{x}_0) \exp\left\{ -i2\pi\mathbf{x}_0 \times \frac{\mathbf{x}' + [M_z(\mathbf{m}p - \mathbf{x}) - \mathbf{m}p]}{\lambda g} \right\} \mathrm{d}^2\mathbf{x}_0 \right|^2, \tag{2}$$

where $\mathbf{m} = (m, n)$ accounts for the indices of the microlenses in the (x, y) directions and p stands for the constant pitch of the microlens array. In Eq. (2) $M_z = -g/(a - z)$ is a magnification factor that depends on depth coordinate z. The so-called generalized pupil function is

$$\mathsf{P}_z(\mathbf{x}_0) = p(\mathbf{x}_0) \exp\left[i \frac{\pi}{\lambda} \left(\frac{1}{a - z} - \frac{1}{a} \right) |\mathbf{x}_0|^2 \right]. \tag{3}$$

This function accounts for the pupil function of the microlenses $p(\mathbf{x}_0)$ together with the phase modulation due to the defocus errors. Note that in principle the main focus of our research is not the intensity distribution at the aerial pickup plane but the distribution at the pickup-device plane. Note, however, that since such a distribution is a uniformly scaled version of the one in Eq. (2), it is correct to base our study on such an equation.

Assuming nonsignificant overlapping between the elemental diffraction spots provided by the different microlenses, Eq. (2) can be rewritten in a quite good approximation as the 2D convolution between the

properly scaled and shifted 2D Fourier transform of $\mathsf{P}_z(\mathbf{x}_0)$ and a sampling function, that is,

$$H_\lambda(\mathbf{x}'; \mathbf{x}, z) = \left|\tilde{\mathsf{P}}_z\left(\frac{\mathbf{x}' - M_z\mathbf{x}}{\lambda g}\right)\right|^2 \otimes \sum_{\mathbf{m}} \delta[\mathbf{x}' - \mathbf{m}p(1 - M_z)]. \quad (4)$$

Let us consider now the overall light proceeding from the surface object. In this case the intensity distribution in the pickup plane is obtained as a weighted superposition of the diffraction spots provided by any point of the surface object, namely,

$$\begin{aligned} I_\lambda(\mathbf{x}') &= \int R(\mathbf{x})\delta[z - f(\mathbf{x})]H_\lambda(\mathbf{x}'; \mathbf{x}, z)\mathrm{d}^2\mathbf{x}\mathrm{d}z \\ &= \int R(\mathbf{x})H_\lambda[\mathbf{x}'; \mathbf{x}, z \\ &= f(\mathbf{x})]\mathrm{d}^2\mathbf{x}. \end{aligned} \quad (5)$$

Note that function $H_\lambda(\cdot)$ explicitly depends on $\mathbf{x}' - M_z\mathbf{x}$, that is,

$$H_\lambda(\mathbf{x}'; \mathbf{x}, z) = H_\lambda[\mathbf{x}' - M_z\mathbf{x}; 0, z] \equiv \mathsf{H}_\lambda(\mathbf{x}' - M_z\mathbf{x}; z). \quad (6)$$

Then Eq. (5) can be rewritten as

$$I_\lambda(\mathbf{x}') = \int R(\mathbf{x})\mathsf{H}_\lambda[\mathbf{x}' - M_z\mathbf{x}; z = f(\mathbf{x})]\mathrm{d}^2\mathbf{x}. \quad (7)$$

Although Eq. (7) seems to represent a 2D convolution, it does not. This is because function $\mathsf{P}_z(\mathbf{x}_0)$ strongly depends on the axial position of the corresponding surface points. In other words, function $\mathsf{H}_\lambda(\cdot)$ is different for different values of z. Besides, factor M_z also depends on z, and therefore parts of the object at a different depth are magnified in a different way. Consequently the impulse response is different at any depth. This fact implies that the pickup system is not linear and shift invariant. Therefore neither the point-spread function nor the optical transfer function could be rigorously defined.

As seen above, the acquired image is composed of an array of elemental images of the surface object, each obtained from a different viewpoint. Let us now focus on the elemental image produced by one of the microlenses, for example, the one in the center of the microlens array. (This selection does not subtract any generality from our study.) The intensity distribution of such an elemental image is given by

$$I_\lambda{}^0(\mathbf{x}') = \int R(\mathbf{x})\mathsf{H}_\lambda{}^0(\mathbf{x}' - M_z\mathbf{x}; z)\mathrm{d}^2\mathbf{x}, \quad (8)$$

where

$$\mathsf{H}_\lambda{}^0(\mathbf{x}'; z) = \left|\tilde{\mathsf{P}}_z\left(\frac{\mathbf{x}'}{\lambda g}\right)\right|^2. \quad (9)$$

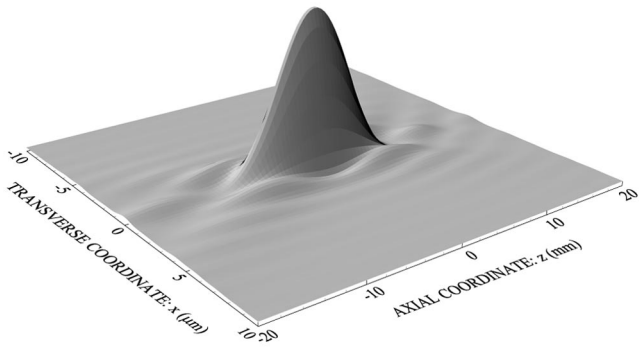

Fig. 2. Three-dimensional plot of the meridian section of function $\mathsf{H}_\lambda{}^0(r, z)$ when the pupil of the microlens is a circle of diameter ϕ. The parameters for the calculation are $\phi = 2.0$ mm, $f = 5.0$ mm, $\lambda = 0.5$ μm, and $a = 100$ mm.

We assume that the pupil of each microlens is a circle with diameter ϕ. In such a case it is convenient to express Eq. (9) in cylindrical coordinates:

$$\mathsf{H}_\lambda{}^0(r, z) = \left|\int_0^{\phi/2} p(r_0)\exp\left[i\,\frac{\pi}{\lambda}\,\frac{z}{a(a - z)}\,r_0{}^2\right] \times J_0\left(2\pi\,\frac{rr_0}{\lambda g}\right)r_0\mathrm{d}r_0\right|^2. \quad (10)$$

3. Influence of the Amplitude Modulation of the Microlenses

As stated above, the function in Eq. (10) does not represent the microlens 3D PSF. Conversely it accounts for the intensity responses, at the pickup plane, to a point source that is axially displaced in the neighborhood of the reference plane. In Fig. 2 we represent in a 3D plot of a meridian section of Eq. (10). The parameters for the calculation are $\phi = 2.0$ mm, $f = 5.0$ mm, $\lambda = 0.5$ μm, and $a = 100$ mm. Note that, because of the low value for the NA lens, the axial extent of H_0 is much higher than the lateral extent. In the $z = 0$ section we can recognize the Airy disk pattern, whose extent determines the lateral resolution of the system. Along the optical axis, $\mathbf{x} = 0$, we find a sinc^2 modulation whose extent determines the depth of field. Accordingly the lateral resolution of an imaging system is determined by the radius of the first zero ring of $\mathsf{H}_\lambda{}^0(r, 0)$. From Fig. 2 we find that in this case the resolution limit, as defined by Rayleigh, is 1.61 μm, if measured in the pickup plane, or 30.6 μm, if evaluated in the reference-object plane. The depth of field is usually evaluated by means of the so-called Rayleigh range, which is defined as the extent of the axial interval in which $\mathsf{H}_\lambda{}^0(0, z)$ is higher than $\sqrt{2}/2$ times its maximum value.[22] In this case the Rayleigh range is -3.3 mm $< z <$ 3.1 mm. Note that the pixel size of the capture device is a factor that strongly influences the depth of focus and resolution. However, in our calculations we considered that the pixels are sufficiently fine.

To illustrate the limitations in the depth of field of

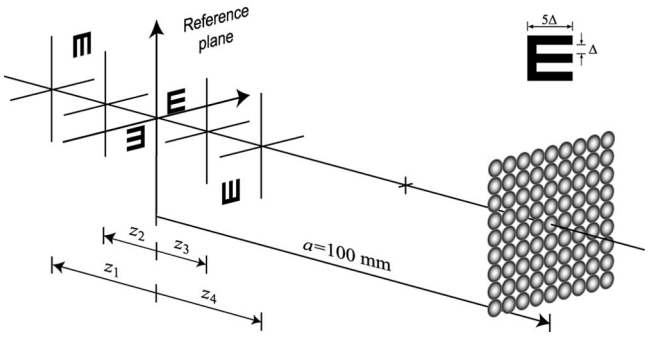

Fig. 3. Schematic, not to scale, of the integral-imaging numerical experiment. The size of the legs of the charts used in our experiments is $\Delta = 51$ μm, which is approximately twice the Rayleigh resolution limit.

an integral-imaging system, we performed a numerical experiment in which we obtained the elemental images of a computer-synthesized object. Since the aim of the experiment was to appreciate the improvement in the depth of field, we selected as the object the Snellen **E** tumbling chart, which is usually used to grade resolution and defocus errors in the visual optics. In the experiment the **E** patterns are positioned side by side and are longitudinally located at $z_1 = -10.0$ mm, $z_2 = -5.0$ mm, $z_3 = +4.6$ mm, $z_4 = +8.3$ mm as depicted in Fig. 3. Note that the axial positions were not symmetric about the reference plane but correspond to the same amount of defocus as defined in terms of the well-known defocus coefficient $\omega_{20} = z\phi^2/2\lambda a(a - z)$.[23] The elemental images were calculated according to Eq. (7).

The images captured from nine different views are shown in Fig. 4. In Fig. 5 we show an enlarged image of the central element $\mathbf{m} = (0, 0)$. It is clear from Fig. 5 that the images of the **E** patterns in z_1 and z_4 are highly blurred. Note that, since the imaging system is not telecentric,[24] the images corresponding to planes with the same modulus of ω_{20} but a different sign are different. This is due to the different scale of defocused images. Because of this effect, the elemental image of the **E** patterns located at z_1 is much more blurred than the elemental image corresponding to the **E** pattern at z_4. It is noticeable that in the case of the pattern at z_1 one can hardly distinguish the original orientation of **E** in the elemental image.

4. Binary Amplitude Modulation Technique

The easiest way to improve the depth of field of the capture setup is by reducing the NA of the microlenses. However, such an improvement is accompanied by a proportional deterioration of lateral resolution. This problem can be overcome by use of amplitude-modulation techniques. Specifically we propose the use of binary amplitude modulators. Such a kind of modulator has been successfully applied to improving the performance of other 3D imaging techniques such as confocal microscopy[25] or multiphoton scanning microscopy.[26] The technique, which is simple albeit surprisingly effective, has never been proposed in the context of integral imaging. It consists of obscuring the central part of each microlens. Such an obscuration allows the secondary Huygens wavelets proceeding from the outer part of the lenses to interfere constructively in an enlarged axial range. Then, by simply placing an opaque circular mask of diameter $D = \delta\phi$ (with $0 < \delta < 1$) just behind each microlens, one can

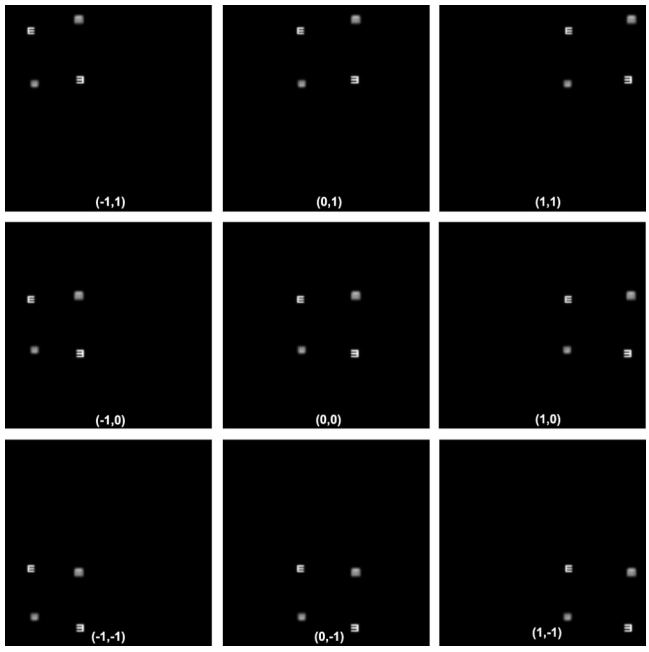

Fig. 4. Two-dimensional elemental images of the tumbling chart captured from nine different views. At any element image we do not show the entire field of view but only a portion of 0.4 mm × 0.4 mm centered at the corresponding optical axis.

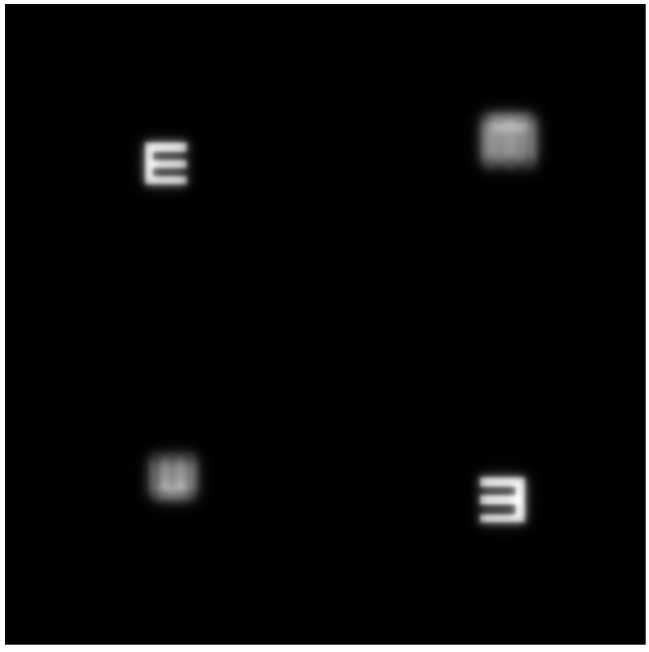

Fig. 5. Enlarged view of the central elemental image in Fig. 4.

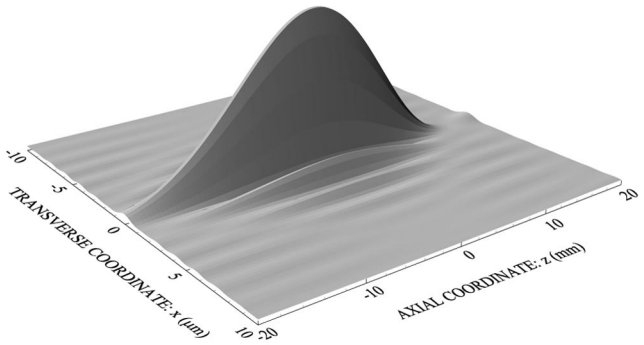

Fig. 6. Three-dimensional plot of the meridian section of function $H_\lambda^0(r, z)$ when the amplitude transmittance of the microlens is modulated with a binary mask of obscuration ratio $\delta = \sqrt{2}/2$. As in the previous experiment the parameters for the calculation are $\phi = 2.0$ mm, $f = 5.0$ mm, $\lambda = 0.5$ μm, and $a = 100$ mm.

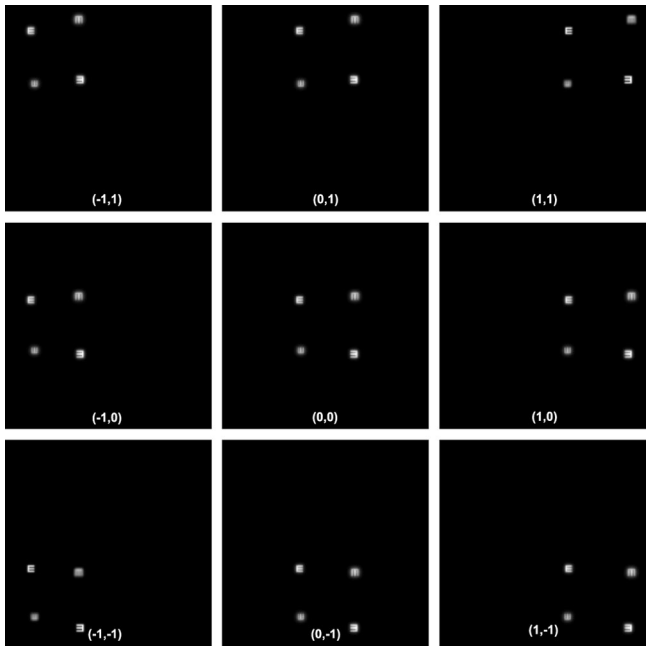

Fig. 7. Two-dimensional elemental images captured with the amplitude-modulated microlens array. At any element image we do not show the entire field of view but only a portion of 0.4 mm × 0.4 mm centered at the corresponding optical axis.

increase the focal depth of the microlens array. It is known that the higher the value of the obscuration ratio δ, the broader the axial intensity spot. In an ideal case, one could obtain an infinite depth of focus by approaching the value of δ to the unity. However, such a situation is not convenient from an experimental point of view, because the higher the value of δ the smaller the light efficiency of the system. On the other hand, if one works with only the outermost part of the lenses, the optical aberrations of the system dramatically increase. For these reasons we propose using the binary modulator of obscuration ratio $\delta = \sqrt{2}/2$. This modulator has a light efficiency of 50% and doubles the depth of focus of the system.

In Fig. 6 we plotted a meridian section of function $H_\lambda^0(r, z)$ for the case of amplitude modulation with obscuration ratio $\delta = \sqrt{2}/2$. In this case the Rayleigh resolution limit is 22.3 μm (as evaluated in the reference plane), whereas the depth of field interval is $-6.8 \text{ mm} < z < +6.0 \text{ mm}$. If we compare these results with those obtained with the nonmodulated setup (see Fig. 2), we find that the depth of field has been doubled and that the 2D density of resolved points has been increased by a factor of 1.85. We can evaluate the power of our technique in terms of a recently defined figure of merit for integral-imaging systems: the product of the depth of focus and the resolution square (PDRS).[19] We find that the use of binary amplitude modulation allows the PDRS to increase by a factor of 3.7.

Also in this case we have performed the numerical experiment with the same Snellen **E** tumbling chart as in Section 3. The nine elemental images when amplitude-modulated lenslets are used are shown in Fig. 7. The enlarged view of the central elemental image $\mathbf{m} = (0, 0)$ is shown in Fig. 8. By comparing Figs. 5 and 8, one observes noticeable improvement in the depth of field provided by the amplitude-modulation, phase-elements method. Note, on the other hand, that the images of objects at z_2 and z_3 are slightly more blurred than those obtained with the nonmodulated architecture. This fact seems to contradict the statement that the binary modulation improves the lateral resolution, as defined by Rayleigh, for objects placed at any depth z. Take into account, however, that the Rayleigh resolution limit is defined for point objects, and therefore it does not hold in case of more elaborate objects. In such a case the use of

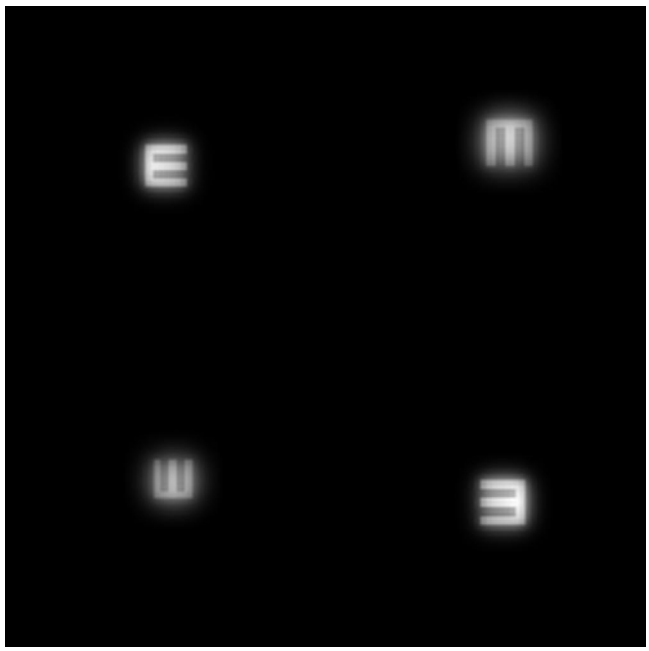

Fig. 8. Enlarged view of the central elemental image in Fig. 7. Note that, strictly speaking, the light intensity of these images should be half of that of the images in Fig. 5. This affect does not appear in the figures because they are normalized differently.

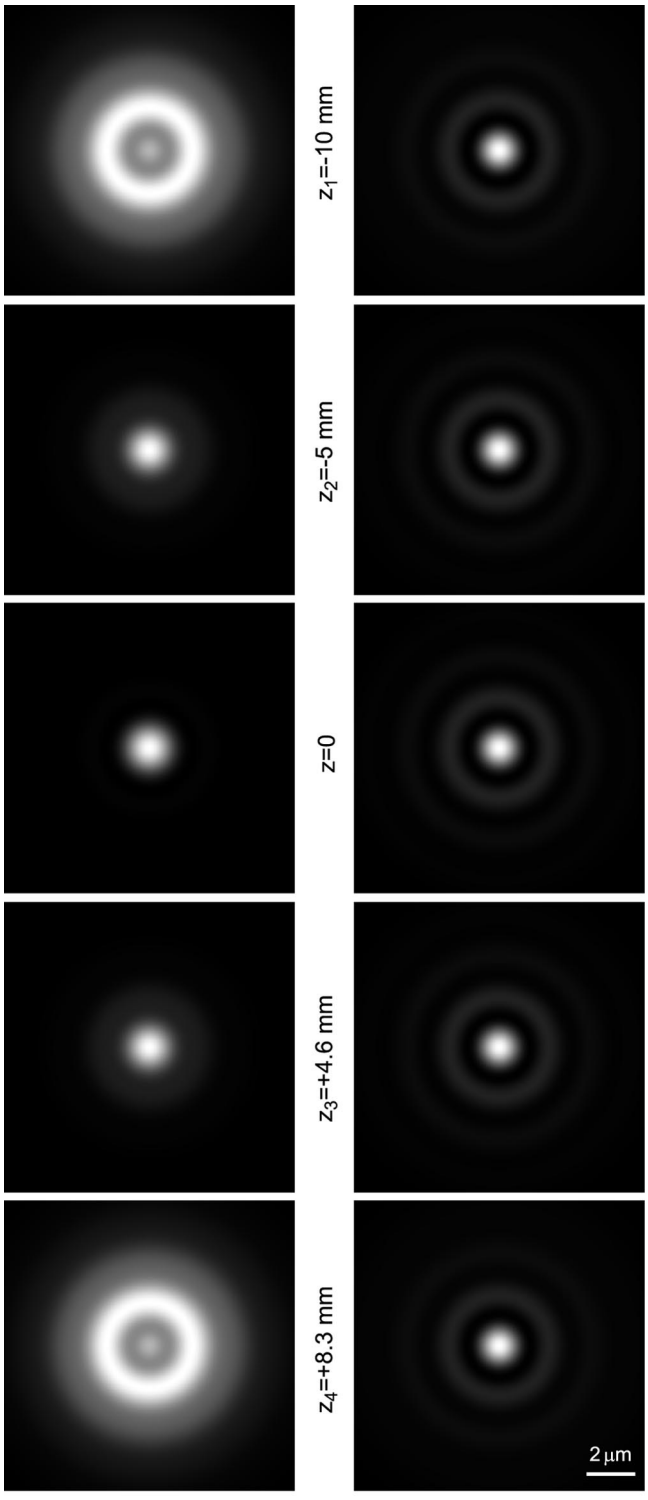

Fig. 9. Cross sections of function $H^0(\mathbf{x}', z)$ corresponding to the nonmodulated lenses and the amplitude-modulated lenses.

binary amplitude modulation improves lateral resolution in a very large range of depth positions but produces a slight worsening for low values of depth coordinate z.

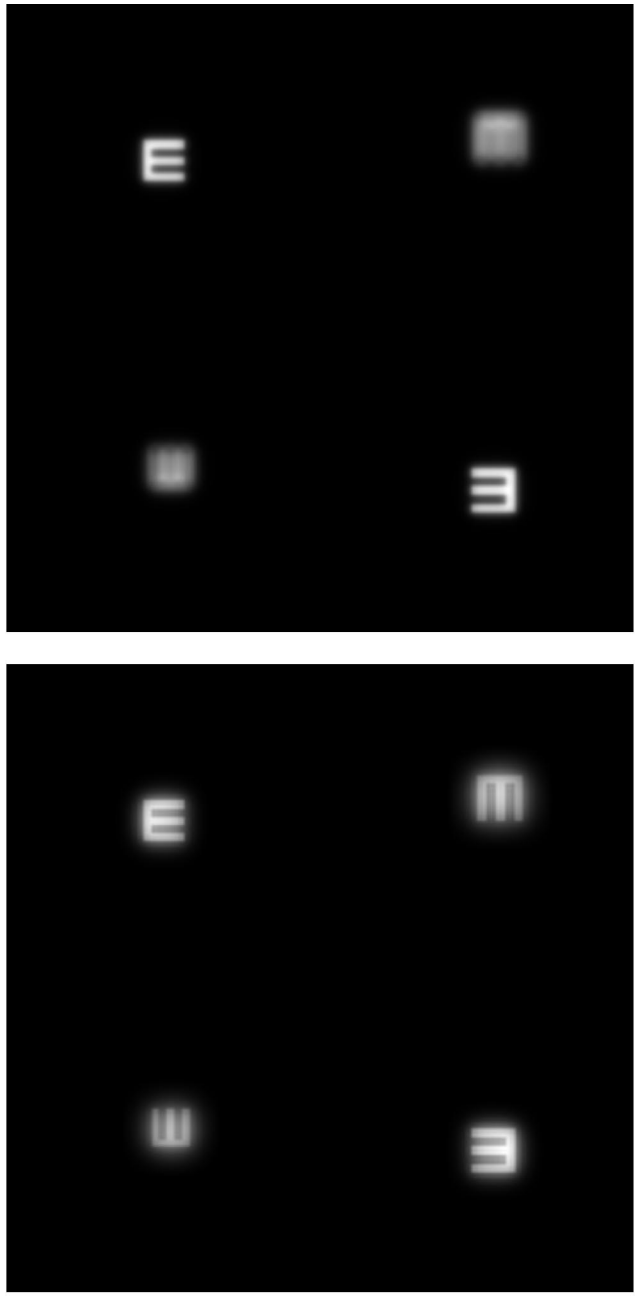

Fig. 10. Enlarged view of the central elemental image obtained by taking into account the polychromatic nature of the illumination: Top, image obtained with the nonmodulated lens; bottom, image obtained with the amplitude-modulated lens.

5. Polychromatic-Illumination Case

In this section we apply our formalism to a more realistic situation in which we consider that the surface object is illuminated by a white-light source. In this case the intensity distribution captured by the CCD corresponding to the central elemental image is given by

$$I^0(\mathbf{x}') = \int_0^\infty V(\lambda) I_\lambda{}^0(\mathbf{x}') \mathrm{d}\lambda, \tag{11}$$

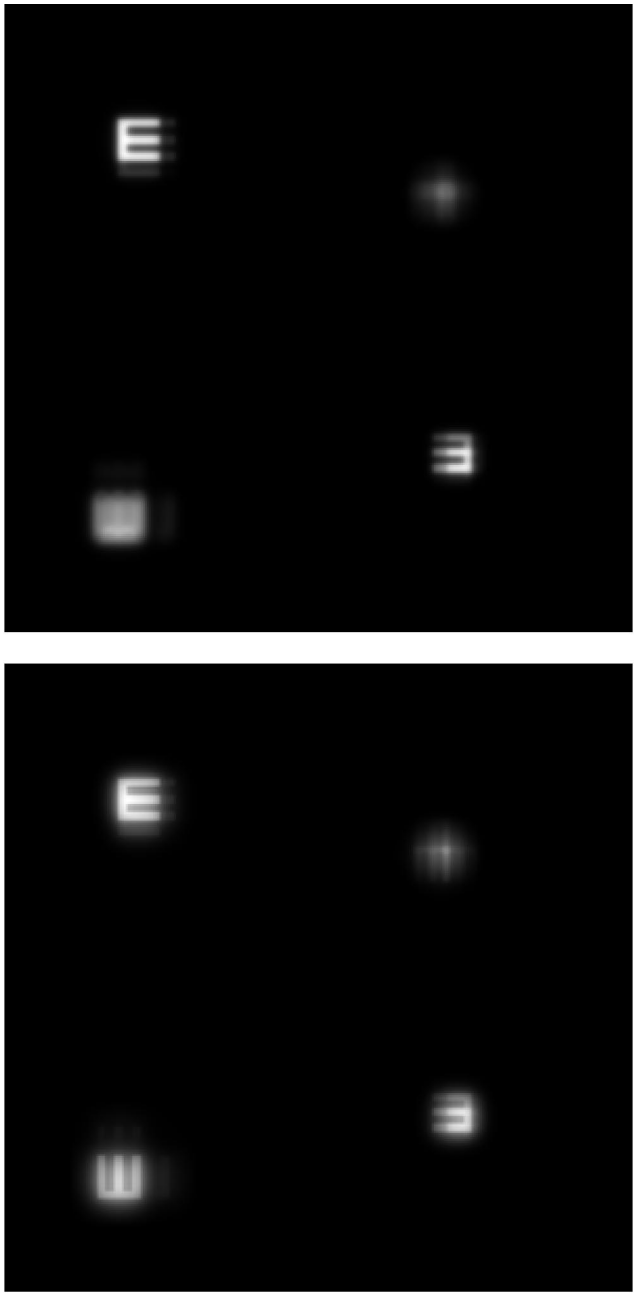

Fig. 11. Reconstructed image obtained from the simulated elemental images obtained with, top, the nonmodulated pickup lenslet array and, bottom, the binary-modulated pickup lenslet array.

where $I_\lambda{}^0(\mathbf{x}')$ was defined in Eq. (8) and function $V(\lambda)$ accounts for the normalized spectral sensitivity of the CCD. Note that Eq. (11) can be rewritten as

$$I^0(\mathbf{x}') = \int R(\mathbf{x}) \mathrm{H}^0(\mathbf{x}' - M_z\mathbf{x}; z) \mathrm{d}^2\mathbf{x}, \qquad (12)$$

where

$$\mathrm{H}^0(\mathbf{x}'; z) = \int_0^\infty V(\lambda) \mathrm{H}_\lambda{}^0(\mathbf{x}'; z) \mathrm{d}\lambda. \qquad (13)$$

Equation (13) represents the response of the CCD to a white-light point source that is axially displaced a distance z from the reference plane. In Fig. 9 we plotted some different cross sections of function $\mathrm{H}^0(\mathbf{x}'; z)$ corresponding to the two cases being studied. The parameters for the calculation were the same as in Figs. 2 and 6, and we have used as function $V(\lambda)$ the spectral sensitivity provided by Apogee, corresponding to the CCD model AP1E. It is clear that also in the case of polychromatic illumination the use of the binary obscuration produces a significant increase in the tolerance of the system to defocus.

In Fig. 10 we performed the same numerical experiment as in Figs. 5 and 8 but now taking into account the polychromatic nature of the illumination. Note that now the images are slightly more blurred than in the monochromatic case, but it is still clear that the amplitude modulation of the microlenses produces a significant enlargement of the depth of field of the integral-imaging system.

To finish with our numerical integral-imaging experiment, we calculated the reconstructed image by simulation with the simulated elemental images. For this numerical reconstruction we considered that the integral image was observed by an eye with a pupil diameter of $\phi_E = 3$ mm, which was placed on the optical axis of the central microlens and at a distance of $l = 300$ mm from the reference plane. The reconstructed images are shown in Fig. 11. Note that we used for the reconstruction, in the two cases being studied, a nonmodulated lenslet array. This is because the use of binary obscurations in the reconstruction setup could produce an important vignetting effect in the image. It is clear that the quality of the reconstructed integral image is much better in the case of the amplitude-modulated system.

6. Conclusions

In summary we have presented a new technique for simultaneously improving both the depth of field and the spatial resolution of the 3D integral-imaging systems. The technique is based on modulating the amplitude transmittance of the microlenses. We have shown that, by simply properly blocking the central part of the microlenses, one can increase the PDRS of an integral-imaging system by 370%. Besides, owing to the simplicity of the proposed technique, which does not imply significant modification of the integral-imaging architecture, this technique could be combined with other techniques[19–21] to produce further improvements in the performance of integral-imaging systems.

M. Martínez-Corral and G. Saavedra gratefully acknowledge financial support from Plan Nacional I+D+I (grant DPI2003-4698), Ministerio de Ciencia y Tecnología, Spain. They also acknowledge financial support from the Generalitat Valenciana, Spain (grant grupos03/227).

References

1. M. G. Lippmann, "Epreuves reversibles donnant la sensation du relief," J. Phys. (Paris) **7,** 821–825 (1908).
2. H. E. Ives, "Optical properties of a Lippmann lenticulated sheet," J. Opt. Soc. Am. **21,** 171–176 (1931).
3. N. A. Valyus, *Stereoscopy* (Focal, London, 1966).
4. R. L. de Montebello, "Wide angle integral-photography: the integram technique," in *Three-Dimensional Imaging*, S. A. Benton, ed., Proc. SPIE **120,** 73–91 (1970).
5. T. Okoshi, *Three Dimensional Imaging Techniques* (Academic, London, 1976).
6. Y. A. Dudnikov, B. K. Rozhkov, and E. N. Antipova, "Obtaining a portrait of a person by the integral photography method," Sov. J. Opt. Technol. **47,** 562–563 (1980).
7. T. Motoki, H. Isono, and I. Yuyama, "Present status of three-dimensional television research," Proc. IEEE **83,** 1009–1021 (1995).
8. M. McCormick and N. Davies, "Full natural colour 3D optical models by integral imaging," in Proceedings of Fourth International Conference on Holographic Systems, Components, and Applications, (Institute of Electrical Engineers, London, 1993), pp. 237–242.
9. H. Arimoto and B. Javidi, "Integral three-dimensional imaging with digital reconstruction," Opt. Lett. **26,** 157–159 (2001).
10. F. Okano, H. Hoshino, J. Arai, and I. Yayuma, "Real time pickup method for a three-dimensional image based on integral photography," Appl. Opt. **36,** 1598–1603 (1997).
11. H. Hoshino, F. Okano, H. Isono, and I. Yuyama, "Analysis of resolution limitation of integral photography," J. Opt. Soc. Am. A **15,** 2059–2065 (1998).
12. T. Naemura, T. Yoshida, and H. Harashima, "3-D computer graphics based on integral photography," Opt. Express **8,** 255–262 (2001), http://www.opticsexpress.org.
13. J.-H. Park, S.-W. Min, S. Jung, and B. Lee, "Analysis of viewing parameters for two display methods based on integral photography," Appl. Opt. **40,** 5217–5232 (2001).
14. L. Erdman and K. J. Gabriel, "High resolution digital photography by use of a scanning microlens array," Appl. Opt. **40,** 5592–5599 (2001).
15. J.-S. Jang and B. Javidi, "Improved viewing resolution of three-dimensional integral imaging by use of nonstationary micro-optics," Opt. Lett. **27,** 324–326 (2002).
16. J.-S. Jang and B. Javidi, "Three-dimensional synthetic aperture integral imaging," Opt. Lett. **27,** 1144–1146 (2002).
17. J. Arai, H. Hoshino, M. Okui, and F. Okano, "Effects on the resolution characteristics of integral photography," J. Opt. Soc. Am. **20,** 996–1004 (2003).
18. A. Stern and B. Javidi, "3-D computational synthetic aperture integral imaging (COMPSAII)," Opt. Express **11,** 2446–2451 (2003), http://www.opticsexpress.org.
19. J.-S. Jang, F. Jin, and B. Javidi, "Three-dimensional integral imaging with large depth of focus by use of real and virtual image fields," Opt. Lett. **28,** 1421–1423 (2003).
20. B. Lee, S.-W. Min, S. Jung, and J.-H. Park, "Computer-generated dynamic three-dimensional display using integral photography adopting Fresnel lenses," in *Algorithms and Systems for Optical Information Processing V*. B. Javidi and D. Psaltis, eds., Proc. SPIE **4471,** 9–17 (2001).
21. J.-S. Jang and B. Javidi, "Large depth-of-focus time-multiplexed three-dimensional integral imaging by use of lenslets with nonuniform focal lengths and aperture sizes," Opt. Lett. **28,** 1924–1926 (2003).
22. A. E. Siegman, *Lasers* (University Science, Saulito, Calif., 1986).
23. A. Stokseth, "Properties of a defocused optical system," J. Opt. Soc. Am. **59,** 1314–1321 (1969).
24. C. J. Zapata-Rodríguez, P. Andrés, M. Martínez-Corral, and L. Muñoz-Escrivá, "Gaussian imaging transformation for the paraxial Debye formulation of the focal region in a low-Fresnel-number optical system," J. Opt. Soc. Am. A **17,** 1185–1191 (2000).
25. C. J. R. Sheppard, "Binary optics and confocal imaging," Opt. Lett. **24,** 505–506 (1999).
26. M. Martínez-Corral, C. Ibáñez-López, G. Saavedra, and M. T. Caballero, "Axial gain resolution in optical sectioning fluorescence microscopy by shaded-ring filters," Opt. Express **11,** 1740–1745 (2003), http://www.opticsexpress.org.